Journal of Institute of Science and Technology, 31(1), 13-24 (2026)
ISSN: 2467-9062 (print), e-ISSN: 2467-9240
https://doi.org/10.3126/jist.v31i1.89170

Research Article

INSAR-BASED CO-SEISMIC DISPLACEMENT MAPPING OF THE 2023 JAJARKOT EARTHQUAKE (M_W 5.7) USING SENTINEL-1A IMAGERY

Nirmal Kafle[1*], Subeg Man Bijukchhen[2]

[1]*Department of Civil Engineering, Khwopa College of Engineering, Bhaktapur, Nepal*
[2]*Post Graduate Department of Earthquake Engineering, Khwopa Engineering College, Bhaktapur Nepal*
**Correspondence: kafle.nirmal@khwopa.edu.np*

(***Received:*** *January 26, 2026;* ***Revised:*** *March 21, 2026;* ***Accepted:*** *April 23, 2026)*

ABSTRACT

On November 3, 2023, Jajarkot district in western Nepal experienced a M_w 5.7 earthquake. The region is seismically active and lies along the Main Himalayan Thrust (MHT). Various slope failures and damages to many masonry structures were reported representing the effects of surface displacement. This study presents the first co-seismic surface displacement analysis of moderate-magnitude earthquake in western Nepal using Sentinel-1A Synthetic Aperture Radar (SAR) data processed through Interferometric SAR (InSAR) workflow. For data processing, Sentinel Application Platform (SNAP) and SNAPHU were employed followed by displacement decomposition in ArcGIS 10.4. The east-west displacement (D_{EW}) ranged from 0.3514 m to -0.2210 m, while the vertical displacement (D_V) varied between 0.4149 m to -0.5149 m. The total ground displacement magnitude was approximately 0.5437-0.5603 m. These findings show that even a moderate-magnitude earthquakes in the Himalayan terrain can produce significant and measurable displacement which highlights the effectiveness of InSAR in post-seismic hazard assessment for remote, data-scarce regions of Nepal.

Keywords: Co-seismic displacement, InSAR, LOS displacement, Sentinel-1A

INTRODUCTION

An earthquake of M_w 5.7 struck Jajarkot district in western Nepal on November 3, 2023. Occurring along the Main Himalayan Thrust (MHT), it also triggered many aftershocks. The intensity of maximum shaking estimated at around VIII on the Medvedev Sponheuer Karnik (MSK) scale (USGS, 2023) resulted in some surface damage and common concern due to its proximity to vulnerable mountainous terrain. Causing widespread destruction within seconds, earthquakes are among the most common devastating geological hazards (Shedlock & Pakiser, 1998). Earthquakes are the result of tectonic movements and they may trigger additional hazards such as tsunamis and landslides (Lay & Kanamori, 1981; Keefer, 1984). Earthquakes do not directly cause fatalities; rather the collapse of poorly designed structures do (Hayes et al., 2024). Prediction of earthquakes accurately has not been possible despite their severe impact (Jordan et al., 2011). Hence, for disaster response and recovery co-seismic assessment becomes crucial (Subedi et al., 2024). The field surveys are time consuming and are sometimes hazardous (Lakshmi & Yarrakula, 2016) in contrast to remote sensing, especially active techniques like Synthetic Aperture Radar (SAR) which provide near real-time monitoring without the peril (Pepe & Calo, 2017).

Interferometric Synthetic Aperture Radar (InSAR) has emerged as a powerful remote sensing technique for delineating co-seismic surface displacement (Wang et al., 2010; Ishwar & Kumar, 2017). It has been utilized rapidly in recent years because of its high precision and wide spatial coverage for mapping ground surface displacement. It compares the phase difference between pairs of images commonly called as master and slave and has been proven effective in detecting millimeter-level surface displacement (Cao et al., 2008). Its capabilities were carried out using Seasat data in the past, where researchers successfully identified sub-centimeter deformation in California's Imperial Valley (Gabriel et al., 1989).

While traditional methods like triangulation and trilateration, are often tedious, uneconomic, and not practical for post-disaster assessment (Yarrakula & Suresh, 2018). InSAR has the advantage of wide-area coverage without extensive field intervention. This technique got popularity when it was successfully applied in mapping tectonic deformation caused by the 1992 Landers earthquake (Massonnet et al., 1993) and deformation mapping has been key to co-seismic

assessment since then (Briole et al., 1997). During several earthquakes around the world InSAR's practical value in disaster assessment was utilized properly. Sentinel-1 data were used to assess the effects of the April 16, 2016 Pedernales earthquake *Mw* 7.8 in Ecuador (Bejar-Pizarro et al., 2018). InSAR data was used to conclude that the inverted co-seismic slip from the 2015 Gorkha earthquake *Mw* 7.3 aftershock was largely confined to a relatively small zone near the epicenter, where the maximum displacement reached around 3 meters (Zhou et al., 2016). These findings supported the integration of this technology into emergency response and decision-making process. Nevertheless, InSAR is not without limitations. During displacement measurement, issues such as phase decorrelation, atmospheric noise, and data voids can produce errors (Bürgmann et al., 2000). Mountainous or forested terrains often lead to geometric distortions, which reduce coherence and affect data quality (Jebur et al., 2015).

The present study focuses on mapping co-seismic surface displacement caused by the 2023 Jajarkot earthquake using Sentinel-1 SAR data processed in Sentinel Application Platform (SNAP). We followed a complete InSAR workflow from pre-processing and interferogram generation to filtering, phase unwrapping, and finally converting the results into displacement. The resulting maps capture how the ground actually moved during the event and help make sense of the underlying seismotectonic processes.

One of the key advantages of Sentinel-1 is its global coverage, open access, and frequent revisit time, which makes it especially useful for studying earthquakes in remote, data-scarce regions like Nepal. Although Himalayan earthquakes have been studied extensively, this particular event has not yet been explored in detail using InSAR. Here, we not only map the deformation but also break down the line-of-sight (LOS) displacement into vertical and horizontal components. Interpreting these patterns in relation to the Main Himalayan Thrust (MHT) and the regional tectonic setting allows us to better understand how moderate magnitude earthquakes shape the landscape in the western Nepal Himalaya.

Seismotectonic of study area

The study area lies in the Jajarkot and parts of Rukum district located in the western Nepal Himalaya (Fig. 1). The Himalaya formed due to the convergence between the Indian and Eurasian plates (Molnar & Tapponnier, 1975; Tapponnier et al., 1982; DeCelles et al., 2014; Ding et al., 2022) is one of the most seismically active regions in the world with numerous past earthquakes (Sapkota et al., 2013; Rahman et al., 2018; Rahman & Bai, 2018; Kanaujia et al., 2024). The main feature of the region is the Main Himalayan Thrust (MHT), which is also the primary source of large-magnitude earthquakes (Avouac, 2003; Bilham, 2004; Hubbard et al., 2016; Bai et al., 2019 & 2025b; Dal Zilio et al., 2019; Kanaujia et al., 2024). The MHT represents the extension of several major surface faults, mainly the Main Frontal Thrust (MFT), Main Boundary Thrust (MBT), Main Central Thrust (MCT), and the South Tibetan Detachment (STD). Tectonically, the Himalayan belt is subdivided into four geological units: the Sub-Himalaya, Lesser Himalaya, Higher Himalaya, and Tethyan Himalaya (Gansser, 1964; Arita et al., 1984; Yin, 2006; Hubbard et al., 2016).

Western Nepal seismicity is influenced by several secondary fault systems, such as the Tibrikot Fault (Nakata, 1989), Dhaulagiri Southwest Fault (Styron et al., 2009), Bari Gad Fault (Murphy et al., 2010), and the Gurla-Mandhata-Humla Fault also referred to as the Western Nepal Fault System or WNFS (Silver et al., 2015). These fault systems contribute to the occurrence of small to moderate earthquakes in the region (Murphy & Copeland, 2005). The Jajarkot earthquake is a thrust fault earthquake with a dip angle of 21º, which occurred above the MHT and consistent with the ramp structure in the Lesser Himalayan duplex system. The rupture area was 25 km along the strike and 20 km along the dip and the rupture nucleated on the ramp structure of the MHT eventually propagating to shallower depths causing severe damage to the surrounding region (Dhakal et al., 2026).

Geophysical and geological evidence points to a steady buildup of seismic strain in this region, raising concerns about the potential for a large earthquake in the future (Sapkota et al., 2013; Stevens & Avouac, 2015). Parts of this broader system have already ruptured in recent years - the 2015 *Mw* 7.8 Gorkha earthquake broke the eastern section of the seismic gap (Bilham, 2015; Hand & Pulla, 2015), and more recently, the 2025 *Mw* 7.1 Dingri earthquake in southern Xizang, roughly 200 km northeast of the Gorkha rupture zone (Bai et al., 2025a). In contrast, western Nepal has remained relatively quiet since the 1505 event, which makes it particularly concerning segment with high likelihood of future large, potentially devastating earthquakes (Rajendran & Rajendran, 2005). The Jajarkot area falling within the Lesser Himalayan domain is structurally complex due to the presence of imbricated thrust sheets, klippen, and crystalline nappes. The region includes tectonic units of Jajarkot Crystalline Zone and Karnali Crystalline Zone, composed of metamorphic rocks

like schists, gneisses, and quartzites, that have undergone significant deformation during Himalayan orogeny (Shahi et al., 2022). Furthermore, the Jajarkot thrust sheet represents an important tectonic element, reflecting intense folding, thrusting, and inverted metamorphism associated with crustal shortening (Tamang et al., 2025). The topography of the study area ranging from 62 m to 5148 m elevation is composed of deeply incised river valleys to rugged terrain, which aggravate the impact of seismic events (Baruah et al., 2020). Accurate mapping of deformation in such environment becomes imperative to assess landslide risks, infrastructure vulnerability, and long-term strain accumulation.

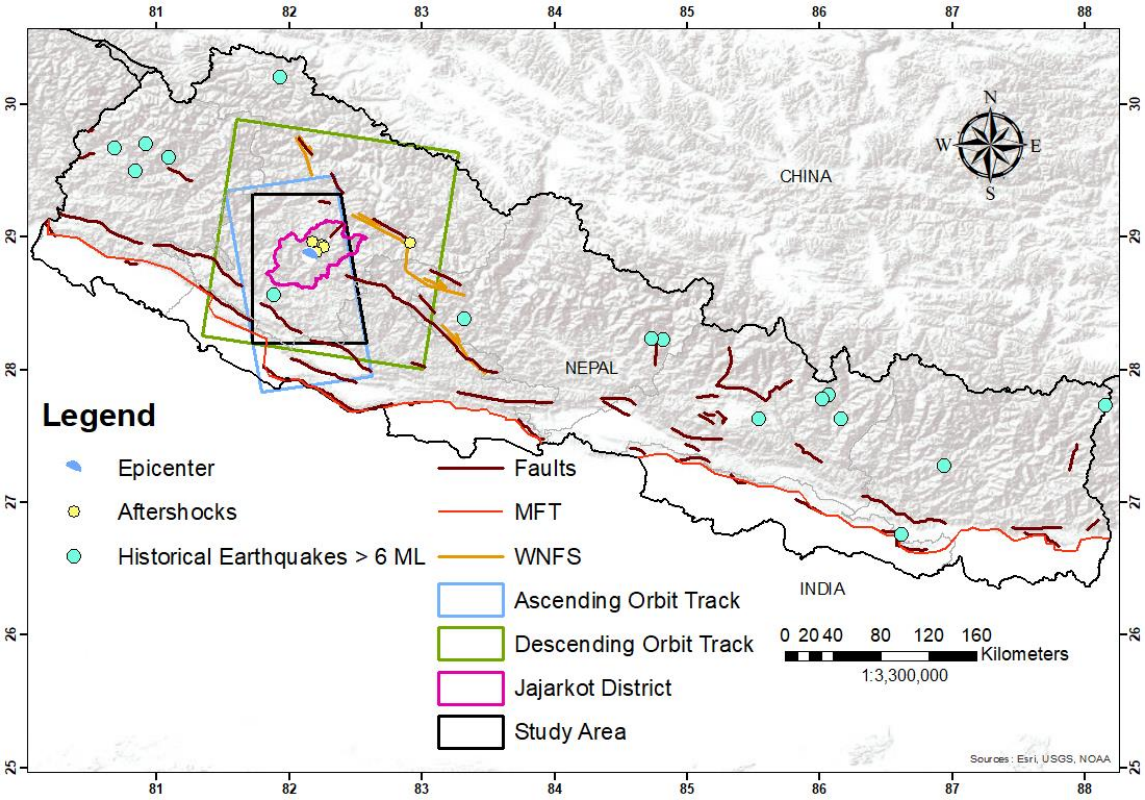

Figure 1. Location of the study area in western Nepal showing the epicenter of Jajarkot earthquake and major tectonic structures (Nakata et al., 1989), including the Main Frontal Thrust (MFT) and Western Nepal Fault System (WNFS) (Silver et al., 2015). Historical earthquake events are compiled from USGS data

MATERIALS AND METHODS

SAR datasets

We utilized Sentinel-1A Interferometric Wide (IW) mode Single Look Complex (SLC) imagery for the analysis employing both descending and ascending descending tracks (Tables 1 and 2). Each pair consisted of pre- and post-event acquisitions with VV (vertical transmit/vertical receive) polarization and similar incidence angles (≈ 46°). The temporal baseline between SAR acquisitions was 12 days for both ascending and descending datasets. Furthermore, both orbit geometries were used to calculate displacement decomposition.

InSAR data processing workflow

The InSAR processing was carried out using ESA's SNAP toolbox and SNAPHU. Figure 2 shows the processing workflow which involves:

1. Orbit correction using Precise Orbit Determination (POD) data,
2. Co-registration and burst selection containing the epicentral region,
3. Interferogram generation and coherence estimation,
4. Goldstein filtering to suppress noise
5. Phase unwrapping in SNAPHU
6. Conversion to LOS displacement, and
7. Range-Doppler Terrain Correction using SRTM 1 Arc-second Digital Elevation Model (DEM).

Firstly, the slave and master Sentinel-1 SLC images were imported into the processing environment and POD files were applied to enhance the geometric accuracy of the satellite data. Subsequently, the IW swath and the specific burst containing the earthquake epicenter were selected through split and subset

process. Finally, accurate co-registration was conducted to align the pre- and post-event SLC images, ensuring pixel-level matching necessary for interferometric analysis.

Table 1. Parameters of sentinel 1A IW SLC descending pass data acquired from abstract metadata

Pass	Master/Slave	Acquisition	Track	Orbit	Angle of incidence (degree)	Swath	Polarization
Descending	Master (Post-event)	06-Nov-23	92	51089	46	IW2	VV
	Slave (Pre-event)	25-Oct-23	92	50914	46	IW2	VV

Table 2. Parameters of sentinel 1A IW SLC ascending pass data acquired from abstract metadata

Pass	Master/Slave	Acquisition	Track	Orbit	Angle of incidence (degree)	Swath	Polarization
Ascending	Master (Post-event)	03-Nov-23	56	51053	46	IW3	VV
	Slave (Pre-event)	22-Oct-23	56	50878	46	IW3	VV

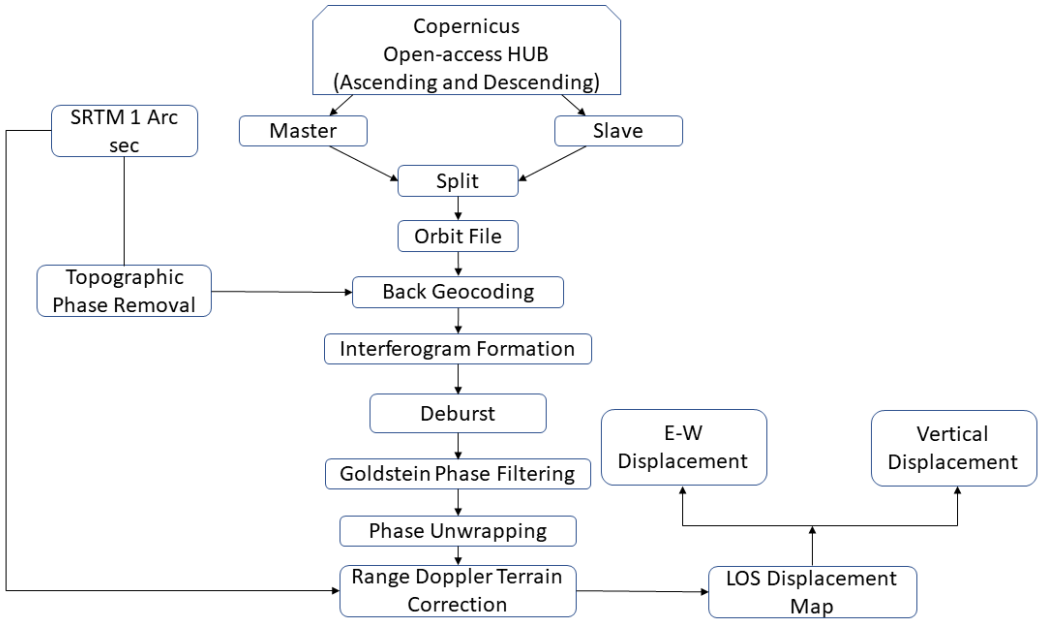

Figure 2. InSAR processing workflow using SNAP and SNAPHU, including co-registration, interferogram generation, filtering, phase unwrapping, and terrain correction

Interferogram was generated using Terrain Observation with Progressive Scans (TOPS) mode processing in SNAP. Interferogram formation was carried out by generating the interference pattern between the pre- and post-event Sentinel-1 images. Phase difference was captured for both descending and ascending passes (Fig. 3 and 4). Goldstein filtering with a coefficient of 0.8 was applied to improve the interferogram quality and reduce noise. Then, phase unwrapping using the SNAPHU algorithm with a statistical cost network flow approach was conducted that transformed the wrapped phase fringes into continuous displacement signals. The coherence threshold was maintained at > 0.3 to mask low-quality pixels. The SRTM 1 Arc-second

(~30 m resolution) DEM was used for topographic phase removal and terrain correction.

The unwrapped phase was then converted to LOS displacement using equation (1) (Hanssen, 2001):

$$d = \frac{\lambda\varphi}{4\pi} \qquad (1)$$

Where, d is the LOS displacement, λ=0.0555 is the wavelength of the Sentinel-1A band sensor, and φ is the unwrapped interferometric phase.

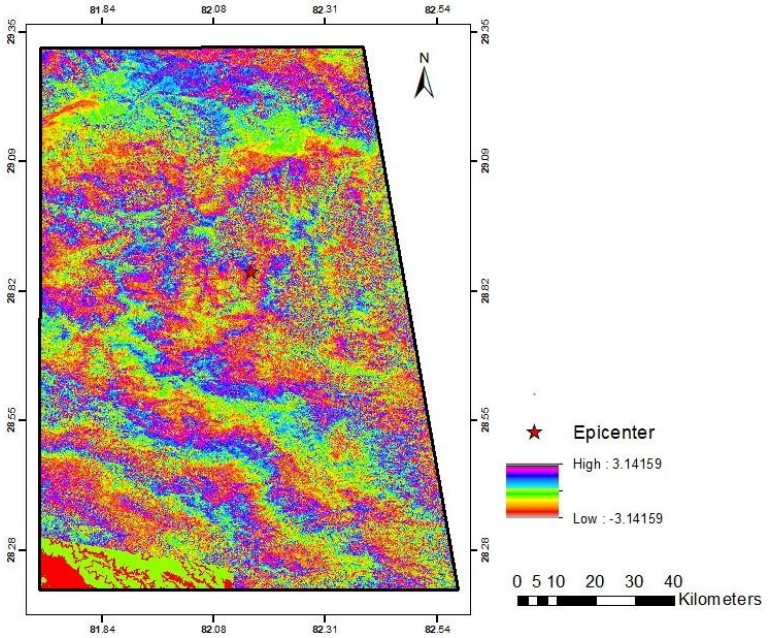

Figure 3. Interferograms from descending and ascending Sentinel-1A SAR data illustrating phase fringes and co-seismic deformation, where color variations represent ground displacement along the radar LOS

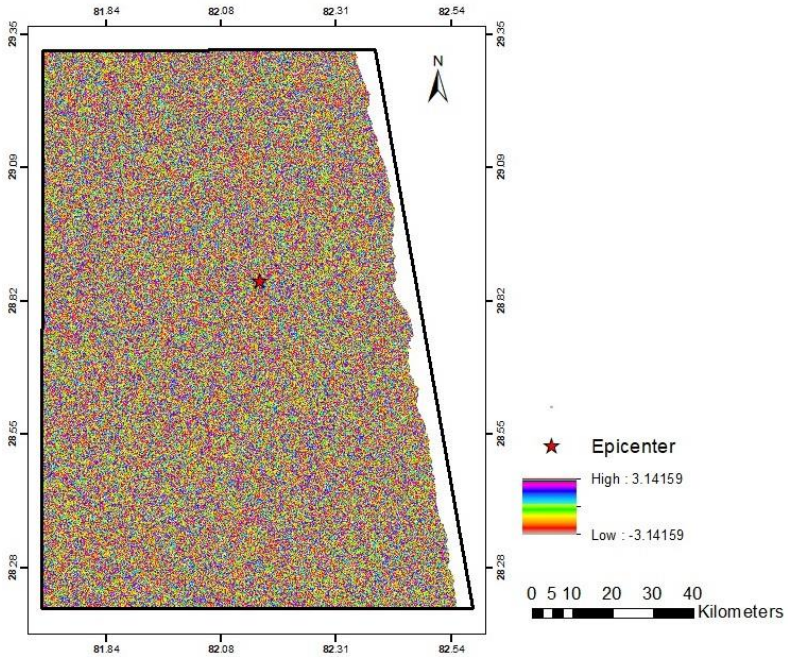

Figure 4. Interferogram over the study area from the ascending orbit of Sentinel-1A. The fringe patterns indicate spatial variation in co-seismic displacement across the study area

Displacement decomposition

The LOS displacement does not directly correspond to three-dimensional surface deformation rather it represents ground motion projected along the radar viewing direction. For better interpretation of co-seismic displacement both the ascending and descending LOS displacement were combined to decompose the displacement into vertical (D_V) and east-west (D_{EW}) components (Fig. 5, 6), using the standard decomposition equations (2 and 3) (Hanssen, 2001):

$$D_V = \frac{D_{asc}+D_{desc}}{2} \quad (2)$$

$$D_{EW} = \frac{D_{asc}-D_{desc}}{2} \quad (3)$$

where, D_{asc} and D_{desc} are LOS displacement of ascending pass and descending pass data respectively.

Using LOS values from both orbits: D_{asc} = 0.766306 m (high), -0.735942 m (low) and D_{desc} = 0.0634908 m (high), -0.293848 m (low), the decomposed displacements were obtained (Table 3). The results indicate that the vertical displacement varied by about 0.93 m, while EW displacement varied by about 0.57 m. The resultant total displacement magnitude was calculated using equation (4) (Hanssen, 2001) yielding a value of approximately 0.5437 m uplift and 0.5603 m subsidence (Table 3):

$$D_{total} = \sqrt{{D_V}^2 + {D_{EW}}^2} \quad (4)$$

Table 3. Decomposed vertical displacement (D_V), east-west displacement (D_{EW}) and resultant total displacement derived from ascending and descending Sentinel-1 SAR data values

Case	$\boldsymbol{D_V}$ **(m)**	$\boldsymbol{D_{EW}}$ **(m)**	$\boldsymbol{D_{TOTAL}}$ **(m)**
High	0.4149	0.3514	0.5437
Low	-0.5149	-0.2210	0.5603

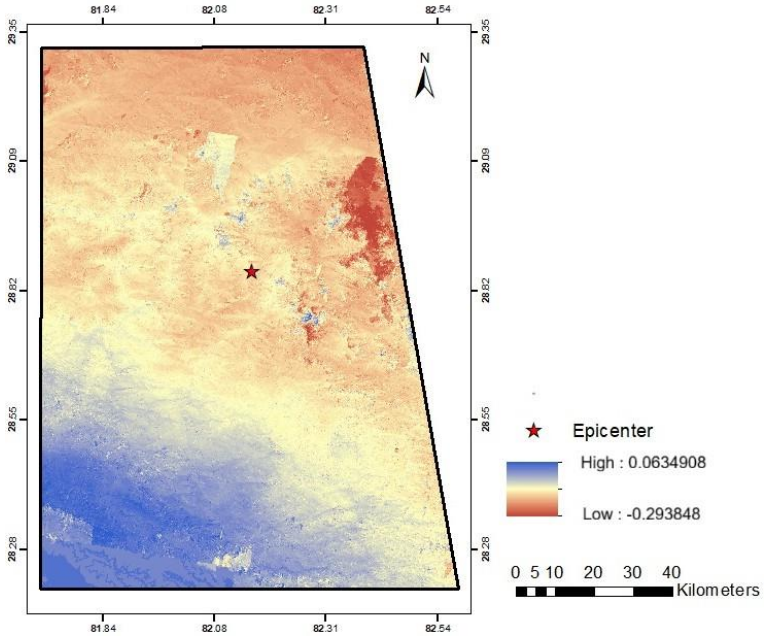

Figure 5. LOS displacement map derived from descending orbit data. Positive values indicate motion toward the satellite, while negative values represent motion away from the satellite. Displacement is shown in meters

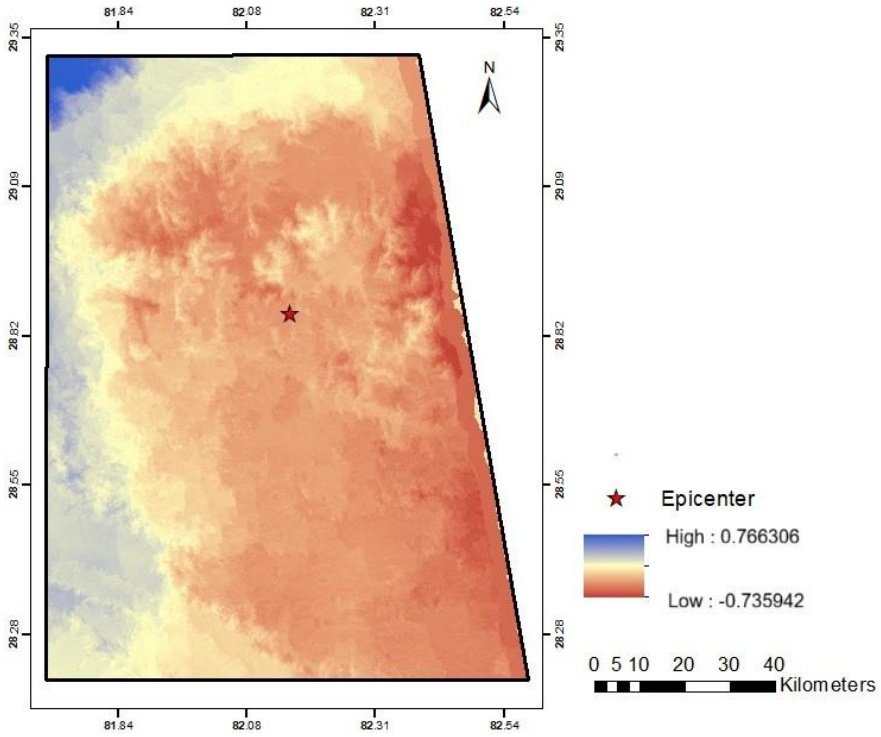

Figure 6. LOS displacement map obtained from ascending data, illustrating ground deformation patterns associated with the earthquake. Color scale represents displacement in meters

RESULTS AND DISCUSSION

The InSAR analysis indicate a distinct co-seismic deformation centered in proximity to the epicenter. The LOS displacement maps (Fig. 5, 6) illustrate an uplift on one flank and subsidence on the opposite, consistent with the thrust-faulting motion along the MHT. Coherence values were 0.93 in stable areas, confirming reliable interferometric signal quality, while vegetated and steep slopes showed minor decorrelation.

A vertical uplift of 0.4149 m and subsidence of -0.5149 m suggest near-surface rupture propagation (Fig. 7). Corresponding east-west motion ranging from 0.3514 m (eastward) and -0.2210 m (westward) indicates lateral displacement probably pertinent to the fault dip and propagation direction (Fig. 8). This reflects horizontal shortening related to the plate convergence. The observed resultant displacement magnitude falls within the range of typical co-seismic motions of M_W 5.5 to 6.5 Himalayan earthquakes (Yarrakula et al., 2018; Jasir et al., 2024**).**

The observation of the co-seismic displacement suggests a shallow seated thrust fault mechanism. This is likely associated with MHT and its imbricate splay faults. The asymmetry in vertical displacement suggests a dipping fault plane with shallow rupture propagation. Despite being a moderate-magnitude earthquake, the shallow rupture propagation allows the surface deformation to be captured by InSAR. The displacements show substantial agreement with post-earthquake field reconnaissance and reporting of slope failures and structure damage (Subedi et al., 2024) carried out in the area.

The displacement pattern calculated in this study, generally aligns well with the tectonic framework of the Nepal Himalaya. When compared to larger Himalayan events like the 2015 Gorkha earthquake, though the displacement of the event is smaller, the overall pattern of deformation is similar, suggesting that the same underlying tectonic processes are at work across the region. These results demonstrate that earthquakes of this scale can still generate a significant surface displacement in the Himalaya due to shallow fault geometry and complex tectonic structures. It can be concluded that in the absence of ground-based observations, InSAR provides valuable insights and means for quantifying co-seismic ground movement at a regional scale. The resulting geocoded displacement map supports co-seismic damage assessment in data-scarce region like the Nepal Himalaya. The findings have important implications for seismic hazard assessment, particularly in identifying zones of strain accumulation and potential landslide triggering in mountainous terrain.

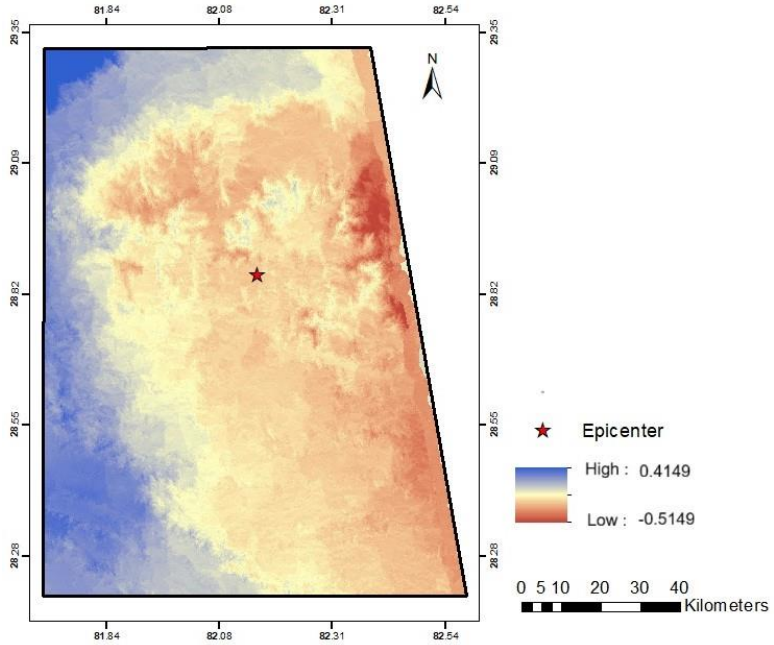

Figure 7. Vertical co-seismic displacement map derived from InSAR analysis. Red indicates uplift (positive displacement), while blue indicates subsidence (negative displacement). The displacement scale is shown in meters

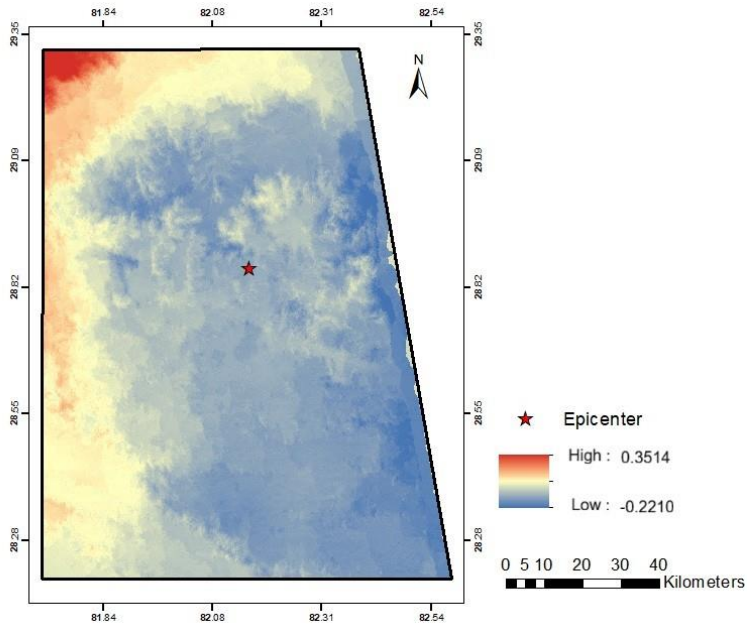

Figure 8. East-West component of co-seismic surface displacement. Positive values (red) indicate eastward movement, while negative values (blue) indicate westward movement. Displacement is shown in meters

CONCLUSION

This study presents the first InSAR-based seismic deformation analysis of western Nepal. It highlights the applicability and effectiveness of Sentinel-1A-based InSAR techniques for mapping co-seismic surface deformation associated with a moderate-magnitude earthquake. The results demonstrate that even moderate earthquakes in the Himalaya can generate measurable ground movement due to shallow thrust faulting along the MHT. Furthermore, the SNAP and SNAPHU workflow enable the generation of high-resolution LOS displacement maps. The findings highlight the potential of InSAR as a rapid and effective tool for seismic hazard assessment in

mountainous regions and provides an improved understanding of tectonic deformation in western Nepal.

ACKNOWLEDGMENTS

The authors are grateful to the Principal and R&D Unit Coordinator of Khwopa College of Engineering for their continuous support throughout the study period.

AUTHORS CONTRIBUTION

Conceptualization: NK, SMB; Methodology: NK, SMB; Data Analysis: NK, SMB; Writing original-draft: NK; Writing Review & Editing: NK, SMB

FUNDING

Small-Scale Research Grant, Khwopa College of Engineering

ORCIDs

Nirmal Kafle:
https://orcid.org/0009-0002-4814-1526
Subeg M. Bijukchhen:
https://orcid.org/0000-0001-7829-8976

CONFLICT OF INTEREST

The authors declare that there are no conflicts of interest regarding the publication of this article

ETHICAL STATEMENT

This manuscript presents original research conducted by the authors. It has not been previously published nor is it currently under consideration for publication in any other journal.

DATA AVAILABILITY STATEMENT

The data supporting the findings of this study are available from the corresponding author upon reasonable request.

SUPPLEMENTARY INFORMATION

None

REFERENCES

Arita, K., Shiraishi, K., & Hayashi, D. (1984). Geology of western Nepal and a comparison with Kumaun, India. *Journal of the Faculty of Science, Hokkaido University, Series IV*, *21*(1), 1–20.

Avouac, J. P. (2003). Mountain building, erosion, and the seismic cycle in the Nepal Himalaya. *Advances in Geophysics*, *46*, 1–80. doi: 10.1016/s0065-2687(03)46001-9

Bai, L., Klemperer, S. L., Mori, J., Karplus, M. S., Ding, L., Liu, H., & Dhakal, S. (2019). Lateral variation of the Main Himalayan Thrust controls the rupture length of the 2015 Gorkha earthquake in Nepal. *Science Advances*, *5*(6). https://doi.org/10.1126/sciadv.aav0723

Bai, L., Chen, Z. W., & Wang, S. J. (2025a). The 2025 Dingri MS6.8 earthquake in Xizang: Analysis of tectonic background and discussion of source characteristics. *Review of Geophysics and Planetary Physics*, *56*(3): 258–263. https://doi.org/10.19975/j.dqyxx.2025-006

Bai, L., Li, H., Chen, Z., Zhan, H., Li, G., Mori, J., & Ding, L. (2025b). Low-angle subduction of the Indian plate and megathrust geometry below the Eastern Himalayas. *National Science Review*, *12*(12). https://doi.org/10.1093/nsr/nwaf460

Baruah, S., Boruah, G. K., Sharma, S., Hoque, W. A., Chetia, T., Dey, C., & Choudhury, S. (2020). Seismic vulnerability assessment of earthquake-prone mega-city Shillong, India using geophysical mapping and remote sensing. *Georisk: Assessment and Management of Risk for Engineered Systems and Geohazards*, *14*(2), 112–127. https://doi.org/10.1080/17499518.2019.1598560

Béjar-Pizarro, M., Álvarez Gómez, J. A., Staller, A., Luna, M. P., Pérez-López, R., Monserrat, O., & Herrera, G. (2018). InSAR-based mapping to support decision-making after an earthquake. *Remote Sensing*, *10*(6), 899. https://doi.org/10.3390/rs10060899

Bilham, R. (2004). Earthquakes in India and the Himalaya: tectonics, geodesy and history. *Annals of Geophysics*, *47*(2–3). https://dx.doi.org/10.4401/ag-3338

Bilham, R. (2015). Raising Kathmandu. *Nature Geoscience*, *8*(8), 582–584. https://doi.org/10.1038/ngeo2498.

Briole, P., Massonnet, D., & Delacourt, C. (1997). Post-eruptive deformation associated with the 1986–87 and 1989 lava flows of Etna detected by radar interferometry. *Geophysical Research Letters*, *24*(1), 37–40. https://doi.org/10.1029/96GL03705

Bürgmann, R., Rosen, P. A., & Fielding, E. J. (2000). Synthetic aperture radar interferometry to measure Earth's surface topography and its deformation. *Annual review of earth and planetary sciences*, *28*(1), 169–209. https://doi.org/10.1146/annurev.earth.28.1.169

Cao, L., Zhang, Y., He, J., Liu, G., Yue, H., Wang, R., & Ge, L. (2008). Coal mine land subsidence monitoring by using spaceborne insar data-a case study in Fengfeng, Hebei province, China. In *XXIst ISPRS Congress Technical Commission VIII*, *37*, 255–262. International Society for Photogrammetry and Remote Sensing (ISPRS).

Dal Zilio, L., van Dinther, Y., Gerya, T., & Avouac, J. P. (2019). Bimodal seismicity in the Himalaya controlled by fault friction and geometry. *Nature Communications*, *10*(1), 48. https://doi.org/10.1038/s41467-018-07874-8

DeCelles, P. G., Kapp, P., Gehrels, G. E., & Ding, L. (2014). Paleocene-Eocene foreland basin evolution in the Himalaya of southern Tibet and Nepal: Implications for the age of initial India-Asia collision. *Tectonics*, *33*(5), 824–849. https://doi.org/10.1002/2014TC003522

Dhakal, S., Bai, L., Song, B., Li, G., Rahman, M. M., Su, H., & Li, L. (2026). Source parameters of the 2023 M L 6.4 Jajarkot earthquake in the western Nepal seismic gap zone. *Earthquake Science*. https://dx.doi.org/10.1016/j.eqs.2026.03.003

Ding, L., Kapp, P., Cai, F., Garzione, C. N., Xiong, Z., Wang, H., & Wang, C. (2022). Timing and mechanisms of Tibetan Plateau uplift. *Nature Reviews Earth & Environment*, *3*(10), 652–667. https://doi.org/10.1038/s43017-022-00318-4

Gabriel, A. K., Goldstein, R. M., & Zebker, H. A. (1989). Mapping small elevation changes over large areas: Differential radar interferometry. *Journal of Geophysical Research: Solid Earth*, *94*(B7), 9183–9191. https://doi.org/10.1029/JB094iB07p09183

Gansser, A. (1964). *Geology of the Himalayas.* Interscience, New York.

Hand, E., & Pulla, P. (2015). Nepal disaster presages a coming megaquake. *Science 348*(6234), 484–485. https://doi.org/10.1126/science.348.6234.484.

Hanssen, R. F. (2001). *Radar interferometry: Data interpretation and error analysis*. Springer.

Hayes, G. P., Baltay Sundstrom, A. S., Barnhart, W. D., Blanpied, M. L., Davis, L. A., Earle, P. S., Field, N., Franks, J. M., Given, D. D., Gold, R. D., Goulet, C. A., Guy, M. M., Hardebeck, J. L., Luco, N., Pollitz, F., Ringler, A. T., Scharer, K. M., Sobieszczyk, S., Thomas, V. I., & Wolfe, C. J. (2024). *US geological survey earthquake hazards program decadal science strategy, 2024–33* (USGS Circular 1544). US Geological Survey. https://doi.org/10.3133/cir1544

Hubbard, J., Almeida, R., Foster, A., Sapkota, S. N., Bürgi, P., & Tapponnier, P. (2016). Structural segmentation controlled the 2015 Mw 7.8 Gorkha earthquake rupture in Nepal. *Geology*, *44*(8), 639–642. https://doi.org/10.1130/G38077.1

Ishwar, S. G., & Kumar, D. (2017). Application of DInSAR in mine surface subsidence monitoring and prediction. *Current Science*, *112*(1), 46–51. https://doi.org/10.18520/cs/v112/i01/46-51

Jasir, M. C. M., Sreejith, K. M., Agrawal, R., & Begum, S. K. (2024). Application of singular spectrum analysis to InSAR time-series for constraining the post-seismic deformation due to moderate- magnitude earthquakes: the case of 2019 M w 6 Mirpur earthquake, NW Himalaya. *Geophysical Journal International*, *239*(1), 637–645. https://doi.org/10.1093/gji/ggae287

Jebur, M. N., Pradhan, B., & Tehrany, M. S. (2015). Using ALOS PALSAR derived high-resolution DInSAR to detect slow-moving landslides in tropical forest: Cameron Highlands, Malaysia. Geomatics, Natural Hazards and Risk, *6*(8), 741–759. https://doi.org/10.1080/19475705.2013.860407

Jordan, T. H., Chen, Y. T., Gasparini, P., Madariaga, R., Main, I., Marzocchi, W., & Zschau, J. (2011). Operational earthquake forecasting: State of knowledge and guidelines for utilization. *Annals of Geophysics*, *54*(4), 315–391. https://doi.org/10.4401/ag-5350

Kanaujia, J., Ravi Kumar, M., Sunilkumar, T. C., Naresh, B., Devi, A., Vijayaraghavan, R., & Solomon Raju, P. (2024). Nature of the Himalayan Seismicity Belt in the Garhwal–Kumaun Segment and its tectonic implications. *Seismological Research Letters*, *95*(4), 2386–2398. https://doi.org/10.1785/0220230005

Keefer, D. K. (1984). Landslides caused by earthquakes. *Geological Society of America Bulletin*, *95*(4), 406–421.

Lakshmi, E. S., & Yarrakula, K. (2016). Monitoring land use land cover changes using remote sensing and GIS techniques: A case study around Papagni River, Andhra Pradesh, India. *Indian Journal of Ecology*, *43*(2), 383–387.

Lay, T., & Kanamori, H. (1981). An asperity model of large earthquake sequences. *Earthquake Prediction: An International Review*, *4*, 579–592. https://doi.org/10.1029/ME004p0579

Massonnet, D., Rossi, M., Carmona, C., Adragna, F., Peltzer, G., Feigl, K., & Rabaute, T. (1993). The displacement field of the Landers earthquake mapped by radar interferometry. Nature, *364*(6433), 138–142. https://doi.org/10.1038/364138a0

Molnar, P., & Tapponnier, P. (1975). Cenozoic Tectonics of Asia: Effects of a Continental Collision. S*cience*, *189*(4201), 419–426. https://doi.org/10.1126/science.189.4201.419.

Murphy, M. A., & Copeland, P. (2005). Transtensional deformation in the central Himalaya and its role in accommodating growth of the Himalayan orogen. *Tectonics*, *24*(4), TC4012. https://doi.org/10.1029/2004TC001659

Murphy, M. A., Sanchez, V., & Taylor, M. H. (2010). Syncollisional extension along the India–Asia suture zone, south-central Tibet: Implications for crustal deformation of Tibet. *Earth and Planetary Science Letters*, *290*(3-4), 233–243. https://doi.org/10.1016/j.epsl.2009.11.046

Nakata, T. (1989). Active faults of the Himalaya of India and Nepal. https://doi.org/10.1130/SPE232-p243

Pepe, A., & Calò, F. (2017). A review of interferometric synthetic aperture RADAR (InSAR) multi-track approaches for the retrieval of Earth's surface displacements. *Applied Sciences*, *7*(12), 1264. https://doi.org/10.3390/app7121264

Rahman, M., & Bai, L. (2018). Probabilistic seismic hazard assessment of Nepal using multiple seismic source models. *Earth and Planetary Physics*, *2*(4), 327–341. https://doi.org/10.26464/epp2018030

Rahman, M., Bai, L., Khan, N. G., & Li, G. (2018). Probabilistic seismic hazard assessment for Himalayan–tibetan region from historical and instrumental earthquake catalogs. *Earthquakes and Multi-hazards Around the Pacific Rim*, *2*, 161–181. https://doi.org/10.1007/s00024-017-1659-y

Rajendran, C. P., & Rajendran, K. (2005). The status of central seismic gap: a perspective based on the spatial and temporal aspects of the large Himalayan earthquakes. *Tectonophysics*, *395*(1–2), 1939.https://doi.org/10.1016/j.tecto.2004.09.009

Sapkota, S. N., Bollinger, L., Klinger, Y., Tapponnier, P., Gaudemer, Y., & Tiwari, D. (2013). Primary surface ruptures of the great Himalayan earthquakes in 1934 and 1255. *Nature Geoscience*, *6*(1), 71–76. https://doi.org/10.1038/ngeo1669

Shahi, Y. B., Kadel, S., Dangi, H., Adhikari, G., KC, D., & Paudyal, K. R. (2022). Geological exploration, landslide characterization and susceptibility mapping at the boundary between two crystalline bodies in Jajarkot, Nepal. *Geotechnics*, *2*(4), 1059-–083. https://doi.org/10.3390/geotechnics2040050

Shedlock, E., Kaye, M., & Pakiser, L. C. (1998). Earthquakes. US Department of the interior. *US Geological Survey. Denver, Colorado*. Doi: 10.3133/7000006

Silver, C. R., Murphy, M. A., Taylor, M. H., Gosse, J., & Baltz, T. (2015). Neotectonics of the western Nepal fault system: Implications for Himalayan strain partitioning. *Tectonics*, *34*(12), 2494-2513. https://doi.org/10.1002/2014TC003730

Stevens, V.L., & Avouac, J.P. (2015). Interseismic coupling on the main Himalayan thrust. *Geophysical Research Letter 42*(14): 5828–5837. https://doi.org/10.1002/2015gl064845.

Styron, R., Taylor, M., & Murphy, M. (2009). Himalayan orogen-parallel extension from GPS geodesy and structural geology. *5th Intern. Sympos. of Tibetan Plateau: Abst. Beijing*, *52*(53).

Subedi, M., Kc, R., Sharma, K., Misra, J., & Kc, A. (2024). Reconnaissance of the effects of the M W5. 7 (M L6. 4) Jajarkot Nepal Earthquake of 3 November 2023, post-earthquake responses, and Associated lessons to be learned. *Geosciences*, *14*(1), 20. https://doi.org/10.3390/geosciences14010020

Suresh, D., & Kiran Yarrakula, K. Y. (2018). Subsidence monitoring techniques in coal mining: Indian scenario. *Indian Journal of Marine Sciences*, *47*(10), 2047–2053.

Tamang, B. B., Dahal, T. R., Sharma, R., & Dahal, A. (2025). Recent Seismicity of Western Nepal. *Journal of Nepal Geological Society*, *70*(1), 45–51. https://doi.org/10.3126/jngs.v70i1.88327

Tapponnier, P., Peltzer, G. L. D. A. Y., Le Dain, A. Y., Armijo, R., & Cobbold, P. (1982). Propagating extrusion tectonics in Asia: New insights from simple experiments with plasticine. *Geology*, *10*(12), 611–616. https://doi.org/10.1130/0091

United States Geological Survey (USGS). (2023). *M 5.6 - Western Nepal earthquake: ShakeMap and event summary*. U.S. Geological Survey.

Wang, Z., Liu, G., Chen, T. E., Zhang, J., & Huang, G. (2010). Detecting and assessing the land subsidence in coal mining area using PALSAR data based on D-InSAR technique. In *Proceedings of the 2010 2nd International Conference on Computer Engineering and Technology (ICCET), 3*, V3–222–V3–226. IEEE. https://doi.org/10.1109/ICCET.2010.5485843

Yarrakula, K., & Suresh, D. (2018). InSAR-based deformation mapping of earthquakes using Sentinel-1A imagery. *International Journal of Remote Sensing and GIS*, *7*(1), 30–4. https://doi.org/10.1080/10106049.2018.1544289

Yin, A. (2006). Cenozoic tectonic evolution of the Himalayan orogen as constrained by along strike variation of structural geometry, exhumation history, and foreland sedimentation. *Earth-Science Reviews*, *76*(1-2),1–131. https://doi.org/10.1016/j.earscirev.2005.05.004

Zuo, R., Qu, C., Shan, X., Zhang, G., & Song, X. (2016). Co-seismic deformation fields and a fault slip model for the Mw7. 8 mainshock and Mw7. 3 aftershock of the Gorkha-Nepal 2015 earthquake derived from Sentinel-1A SAR interferometry. *Tectonophysics*, *686*, 158–169. https://ui.adsabs.harvard.edu/link_gateway/2016Tectp.686.158Z/doi:10.1016/j.tecto.2016.07.032